Published in final edited form as:

ACS Nano. 2015 May 26; 9(5): 5234–5245. doi:10.1021/acsnano.5b00641.

Real-Time Monitoring of ATP-Responsive Drug Release Using Mesoporous-Silica-Coated Multicolor Upconversion Nanoparticles

Jinping Lai, **Birju P. Shah**, **Yixiao Zhang**, **Letao Yang**, and **Ki-Bum Lee***

Department of Chemistry and Chemical Biology, Institute for Advanced Materials, Devices and Nanotechnology (IAMDN), Rutgers University, Piscataway, New Jersey 08854, United States

Abstract

Stimuli-responsive drug delivery vehicles have garnered immense interest in recent years due to unparalleled progress made in material science and nanomedicine. However, the development of stimuli-responsive devices with integrated real-time monitoring capabilities is still in its nascent stage because of the limitations of imaging modalities. In this paper, we describe the development of a polypeptide-wrapped mesoporous-silica-coated multicolor upconversion nanoparticle (UCNP@MSN) as an adenosine triphosphate (ATP)-responsive drug delivery system (DDS) for long-term tracking and real-time monitoring of drug release. Our UCNP@MSN with multiple emission peaks in UV-NIR wavelength range was functionalized with zinc-dipicolylamine analogue (TDPA-Zn^{2+}) on its exterior surface and loaded with small-molecule drugs like chemotherapeutics in interior mesopores. The drugs remained entrapped within the UCNP-MSNs when the nanoparticles were wrapped with a compact branched polypeptide, poly(Asp-Lys)-*b*-Asp, because of multivalent interactions between Asp moieties present in the polypeptide and the TDPA-Zn^{2+} complex present on the surface of UCNP-MSNs. This led to luminescence resonance energy transfer (LRET) from the UCNPs to the entrapped drugs, which typically have absorption in UV–visible range, ultimately resulting in quenching of UCNP emission in UV–visible range while retaining their strong NIR emission. Addition of ATP led to a competitive displacement of the surface bound polypeptide by ATP due to its higher affinity to TDPA-Zn^{2+}, which led to the release of the entrapped drugs and subsequent elimination of LRET. Monitoring of such ATP-triggered ratiometric changes in LRET allowed us to monitor the release of the entrapped drugs in real-time. Given these results, we envision that our proposed UCNP@MSN-polypeptide hybrid nanoparticle has great potential for stimuli-responsive drug delivery as well as for monitoring biochemical changes taking place in live cancer and stem cells.

Graphical Abstract

*Address correspondence to kblee@rutgers.edu.

Conflict of Interest: The authors declare no competing financial interest.

Supporting Information Available: Schematic description of synthesis, FTIR, ^{1}H NMR, MALDI-TOF-MS, DLS size and zeta potential characterizations of the TDPA-Zn^{2+}-UCNP@MSNs, cell viability and targeted delivery of nanoparticles. This material is available free of charge *via* the Internet at http://pubs.acs.org.

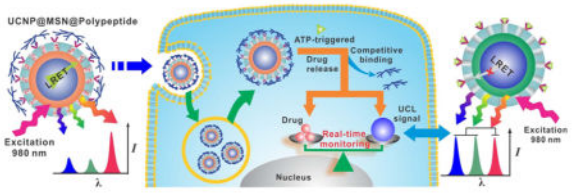

Keywords

upconversion nanoparticle; core–shell nanoparticles; stimuli-responsive drug delivery; real-time monitoring; luminescence resonance energy transfer (LRET)

Spurred by the recent advances made in material science and nanomedicine, “smart” stimuli-responsive drug delivery systems (DDSs) are quickly emerging as a platform of choice for diverse bioapplications including drug delivery and biosensing. By combining the unique properties of advanced nanomaterials with the ability to recognize and adapt in response to a change in their environment, these stimuli-responsive vehicles, which deliver a therapeutic cargo in a spatially, temporally and dosage-controlled manner, improve the bio-pharmaceutical properties of the delivered drugs, reduce their side effects and thereby enhance their clinical utility.[1–5] However, the success of such stimuli-responsive DDS hinges upon three crucial factors: (i) the ability to construct a biocompatible nanocarrier that can retain high loading amounts of the therapeutic molecules, (ii) the development and incorporation of a stimuli-responsive molecular valve into the DDS, which will prevent the premature release of the drug prior to reaching the target location, and (iii) a tracking modality that can allow for real-time monitoring of drug release over extended periods of time. While several bio-compatible and/or biodegradable nanocarriers, such as polymers and liposomes,[6–10] have been explored as DDSs over the past decade, mesoporous-silica nanoparticles (MSNs) have become a powerful delivery vehicle of choice, because of their unique structural features that enable high drug loading and versatility of functionalization.[11–14] Additionally, a variety of endogenous (*e.g.*, pH, enzymes and other biomolecules)[15–18] and exogenous (*e.g.*, light, magnetic field, and temperature)[19–22] stimuli have been explored to construct stimuli-responsive mesoporous DDSs.

Among these, biomolecule-responsive DDSs that bank upon exploiting the physiological and biochemical differences between normal and pathological conditions (*e.g.*, microenvironment in tumors and inflammation sites) have drawn increasing attention owing to their swift and specific triggered drug release.[23–28] One such specific biomolecular stimulus is adenosine triphosphate (ATP), which in addition to being the “molecular unit of currency” for intracellular energy transfer, is also found to be upregulated in cancerous tissues and neurons.[29–31] There is growing evidence that the increased levels of ATP are implicated in many key physiological and pathological processes, such as chemoresistance, uncontrolled tumor growth and synaptic transmission in neurons, thereby making it an interesting target for exploiting the differences between normal and cancer cells, and studying the neuronal system.[32–34]

Another critical component of the stimuli-responsive DDSs is the development of an integrated tracking method having the capability of imaging and monitoring not only the targeted tissues but also the drug release kinetics in a real-time and long-term fashion.[35,36] Such long-term tracking modalities require a highly biocompatible manner, such as noninvasive Raman imaging,[37,38] magnetic resonance imaging,[39–43] and fluorescence microscopy.[17,44–47] Lanthanide-doped up-conversion nanoparticles (UCNPs) have gained tremendous attention in the field of theranostics, molecular imaging and nanomedicine, due to their unique ability of upconverting low-energy near-infrared (NIR) light to high-energy ultraviolet (UV), visible (vis) and NIR light.[5,48–52] The distinctive NIR excitation that enables high penetration depth and low photocytotoxicity (*vs* UV–vis light), as well as other photophysical properties including narrow emission peaks and high photostability, makes UCNPs a promising candidate for developing DDSs with long-term tracking and real-time monitoring capabilities. However, to our knowledge, there have been only a few reports that have demonstrated UCNP-based DDSs showing such capabilities.[40,41]

We herein report the development of a UCNP-based DDS for long-term tracking and real-time monitoring of drug delivery in the response to ATP. As illustrated in Scheme 1, our unique core–shell UCNP@MSN DDS consists of two key components: (i) a UCNP core with distinct emission peaks present in UV to NIR region, when excited at 980 nm, and (ii) a mesoporous silica shell-based "biogate" system for stimuli-responsive (*e.g.*, ATP-responsive) drug release. The biogate for ATP-responsive drug release comprises of a zinc-dipicolylamine analogue (TDPA-Zn^{2+}) immobilized on the exterior surface of the nanoparticle to serve as binding sites for the capping ligands, branched poly-peptides [poly(Asp-Lys)-*b*-Asp] with multiple pendant carboxylate side chains. The high binding affinity of the oligo-aspartate moieties in polypeptide side chains to TDPA-Zn^{2+} moieties on the surface of the UCNP@MSN allows the loaded drugs to remain entrapped inside the mesopores.[53–55] It is expected that, because of the overlap of broad absorption peaks of loaded model drugs [*e.g.*, doxorubicin (DOX) and camptothecin (CPT)] with the multiple sharp emission peaks of UCNP, as well as their close proximity, luminescence resonance energy transfer (LRET) would occur from UCNP (donor) to drug moieties (acceptor), which will result in quenching of the UV–vis emission of UCNPs.[56–58] On the other hand, the NIR emission from our UCNPs will remain constant and can be utilized as a tracking signal. When the stimulus (*e.g.*, ATP in our case) is present, it can lead to a competitive displacement of the surface bound polypeptide by ATP molecule, due to its higher binding affinity to TDPA-Zn^{2+} as compared to the oligo-aspartate in the polypeptide.[59,60] As a result, drugs encapsulated within the mesopores can be released and the LRET signal between the drugs and UCNPs is diminished, which in turn enhances the UV–vis emission of UCNPs. Since the drug release from the mesopores of the UCNPs is accompanied by a simultaneous change in the LRET signal, we can monitor the real-time release of the entrapped drugs over an extended period of time *via* a ratiometric signal using the NIR emission of our UCNPs as an internal reference. Given the importance of ATP in tumor and neural microenvironment, developing such ATP-responsive multifunctional DDS can open new opportunities for cancer therapy and neuroscience.

RESULTS AND DISCUSSION

Synthesis and Characterizations of TDPA-Zn^{2+}-UCNP@MSNs

For the construction of the proposed UCNP@MSN-based DDS, we first synthesized a metallic complex-functionalized UCNP coated with mesoporous silica, TDPA-Zn^{2+}-UCNP@MSN, as shown in Figure 1A. The multicolor UCNP possesses a core–shell structure with a composition of β-$NaYF_4$:Yb^{3+}/Tm^{3+}@$NaYF_4$:Yb^{3+}/Er^{3+}.[61] Such a core–shell structure of UCNP minimizes the cross relaxation of activators, endowing the UCNP with bright emissions shown in UV to NIR region (360, 475, 542 and 656 nm) when excited with a 980 nm NIR laser (Figure 1G). The simultaneous multiplex emission of UCNP in the UV to NIR range is important for the multifunctionality of UCNP@MSN based DDS for two reasons: (1) the individual sharp emission peaks in UV–vis region can serve as an energy donor for LRET to entrapped drugs, such as chemotherapeutics (which typically absorb in the UV–vis range), thereby allowing for real-time monitoring of different drugs; and (2) the NIR emission, on the other hand, remains constant irrespective of the drug molecule present and hence can be used for imaging of the nanoparticle and quantifying the drug release *via* a ratiometric signal (Scheme 1).

Transmission electron microscopic (TEM) analysis revealed that our core–shell UCNP was in the hexagonal phase with a size of 21.5 ± 1.4 nm and 29.2 ± 1.2 nm (n = 100) for the core and shell, respectively (Figure 1B,C). The size of the particle increased to 54.3 ± 3.1 nm (n = 100) after coating with a mesoporous silica shell (Figure 1D,E, and Supporting Information, Figure S2). A tyrosine modified dipicolyl derivative TDPA was successfully grafted to the nanoparticle surface and used as a versatile precursor for chelating different metallic ions such as Zn^{2+} and Cu^{2+} to produce a metallic complex,[62] which further served as binding sites for oligo-aspartate and ATP (Figure S1). The successful grafting of binuclear metallic complex was confirmed using FTIR spectroscopy (Figure S3), UV–vis absorption spectroscopy (Figure 1F) and thermogravimetric analysis (Figure S4). Compared to the UCNP@MSNs, the ligand-functionalized nanoparticles showed the characteristic absorption peaks of TDPA at 280 and 294 nm, which underwent a red shift after chelating with Zn^{2+}. This spectral change for surface-immobilized TDPA is similar to that of free TDPA in aqueous solution (Figure 1F inset), demonstrating the successful formation of metallic complex on nanoparticle surface. Additionally, the TDPA-Zn^{2+}-UCNP@MSNs were well-dispersed in water and retained its characteristic multicolor emissions of UCNP in the range from UV to NIR under 980 nm excitation (Figure 1G), thus indicating feasibility of using these UCNPs for the construction of our proposed multi-functional DDS.

Synthesis and Characterization of Polypeptide, Poly(Asp-Lys)-*b*-Asp

The multivalent coordination between the oligo-aspartate moieties on the polypeptide capping ligands and the zinc-dipicolylamine analogues (Dpa-Zn^{2+}) offer a strong binding affinity with a binding constant of 6.9×10^5 M^{-1} when the peptide consists of four or more aspartate moieties.[53–55] To develop the ATP-responsive molecular valve in our DDS, we synthesized a compact block polypeptide containing oligo-aspartate side chains using *N*-carboxyl anhydride (NCA) based ring opening metathesis polymerization (ROMP) technique with two-generation polymerization.[63–65] This technique allows for extensive

control over the polymerization process, thereby leading to the production of highly monodisperse synthetic polypeptides, while avoiding any unfavorable side reactions. As shown in Figure S5, by varying the molar ratio of the two monomers (*x:y*), Asp(OBzl)-NCA and Lys(Cbz)-NCA during the synthesis of tribranched co-polypeptide backbone (first-generation polymerization, G1), we were able to incorporate different amounts of Lys on the polymer backbone, which subsequently served as an initiator for the second-generation polymerization. Further polymerization with Asp(OBzl)-NCA led to generation of block polypeptides with varying degrees of compactness. The as-synthesized polypeptides were characterized by MALDI-TOF mass spectrum (Figure S6), ^{1}H NMR spectrum (Figure S15–S20), and fluorescamine-based fluorescence analysis (see Supporting Information for more details), for confirming their composition and mean molecular weight. The abundant terminal NH_2 groups of the branched structure allow for facile functionalization of polypeptide, such as labeling with fluorescent dyes and targeting molecules. Using the above-mentioned procedure, we have synthesized four different polypeptides (G2d*i*, *i* = 1, 2, 3 and 4) with various ratios of the three components (*x*, *y*, and *z*) as shown in Scheme 2 and Table 1. The amount of Lys present increased from polypeptide G2d1 and G2d2 to polypeptide G2d3 and G2d4, which indicated an increased number of side chains. Furthermore, the polypeptide G2d2 and G2d4 were designed to have longer branches consisting of eight Asp while the other two peptides, G2d1 and G2d3 consisted of only four Asp. Such changes in the length of the side chains could modulate the structural compactness of the polypeptide and control the binding affinity of the polypeptide to the metallic complex, and as a result influence the selectivity and responsiveness of the DDS to nucleoside-polyphosphates (ATP).

ATP-Responsive Drug Release

The synthetic block polypeptides were expected to bind to the surface of TDPA-Zn^{2+}-UCNP@MSN, because of the multivalent interactions between the oligo-aspartate side chains and the TDPA-Zn^{2+} motifs, with a binding constant as large as 6.9×10^5 M^{-1}.[54] To verify this, we performed the DLS size and ζ-potential characterizations of the UCNPs wrapped with different block polypeptides in aqueous solutions. As shown in Table S1, the hydrodynamic size of TDPA-Zn^{2+}-UCNP@MSN is 65 ± 4 nm with a ζ-potential of +22.5 mV. However, coating with poly-peptide G2d2 and G2d4 increased the hydrodynamic size to 87 ± 6 nm and 91 ± 7 nm respectively, because of the hydration of polypeptides in aqueous solutions. In addition, the G2d2 and G2d4-wrapped nanoparticles were highly negatively charged with a ζ-potential at −25.4 and −32.1 mV, respectively, which could be attributed to the abundant carboxylate side chains of these polypeptides. Taken together, these results demonstrated the successful binding of polypeptides to UCNP surface. After binding to the UCNP surface, the compact multibranched structure of the poly-peptide was expected to entrap the drug molecules inside the pores of nanoparticles effectively. The addition of ATP would then cause competitive displacement of the polypeptides from the UCNP due to higher binding affinity of ATP to the TDPA-Zn^{2+}(4.0×10^7 M^{-1})[59,60] as compared to oligo-aspartate (6.9×10^5 M^{-1})[53–55] and eventually trigger the release of the entrapped drugs.

To test this hypothesis, we used fluorescein as a model drug and prepared block polypeptide (G2d1–G2d4)-wrapped fluorescein-loaded TDPA-Zn^{2+}-UCNP@MSNs as explained earlier.

The amount of dye loaded was calculated to be 13.2 mg fluorescein/g of UCNP@MSN. Thereafter, we showed that the G2d2-wrapped dye-loaded nanoparticles suspended in HEPES buffer solution (pH 7.4, 10 mM) were stable and negligible leakage of fluorescein was observed in the absence of ATP (Figure 2A, curve a), indicating the drug (fluorescein) was entrapped efficiently within the mesopores by the compact block polypeptide. In contrast, the addition of 1 mM ATP led to a rapid release of the fluorescein from the nanoparticles (curve b), with increasing amounts of fluorescein released upon addition of increasing amounts of ATP (curve c, d). These results revealed an ATP-responsive and ATP concentration-dependent drug release property of our UCNPs. Furthermore, we monitored ATP-triggered fluorescein release from TRITC-labeled G2d2-wrapped UCNPs. Comparison of the release profiles of both the TRITC-polypeptide and fluorescein dye clearly showed that the uncapping of polypeptide from UCNP surface occurs prior to fluorescein release from the pores, as can be seen from the rapid increase in TRITC emission (Figure S7). This result demonstrated the release of encapsulated dye was indeed due to the uncapping of the polypeptide as a result of the competitive binding of ATP to the TDPA-Zn^{2+} complex.

It is worth noting that the ATP-responsive drug release profiles of the UCNPs can also be controlled by using different polypeptides shown in Table 1. As shown in Figure 2B, in the presence of the same ATP concentration, UCNPs wrapped by polypeptide with more side chains (G2d3 and G2d4) showed slower and less dye release (curve c and d), as compared to that of polypeptides with less side chains (G2d1 and G2d2, curve a and b). This can be attributed to the increasing number of Asp side chains, which result in higher binding affinity of polypeptides to TDPA-Zn^{2+} on UCNP surface. A similar pattern of drug release was observed in case of polypeptides with longer side chains (G2d4). It showed that G2d4-wrapped UCNP@ MSN has the lowest amount of dye release as well as the slowest release kinetics (curve d) as compared to other polypeptide wrapped nanoparticles, again suggesting that increasing number of Asp moieties can lead to more strongly bound polypeptide and hence slower drug release. Apart from using different polypeptides, the release kinetics could also be modulated by using nanoparticles with different metallic ion complexes. Figure S8 showed the ATP concentrations-dependent drug release profiles of G2d2-wrapped UCNP@MSNs functionalized with TDPA-Zn^{2+} and TDPA-Cu^{2+}. The Cu^{2+}-complex functionalized nano-particle was found to be around 10-fold more sensitive to ATP upon drug release than that of Zn^{2+} complex nanoparticle. Addition of 50 μM ATP to the fluorescein loaded TDPA-Cu^{2+}-UCNP@MSNs induced a remarkable dye release (18%), while 100% dye release was achieved in the presence of 1 mM ATP. This is due to the relatively weak binding affinity between TDPA-Cu^{2+} complex and the polypeptide ($K_{app} < 10^3$ M^{-1}) as compared to that between TDPA-Zn^{2+}complex and polypeptide ($K_{app} = 4.0 \times 10^7$ M^{-1}).[62] These results demonstrate that we can develop a wide variety of ATP-sensitive DDS, where both the metallic complex and the polypeptide can be used to modulate the drug release kinetics in response to ATP.

We further evaluated the specificity of stimulus-responsive uncapping action of our DDS. For this purpose, various phosphate-containing biomolecules including the nucleoside phosphates (ADP, AMP, GTP, UTP, and nucleic acids), proteins (*e.g.*, bovine serum albumin), enzymes (*e.g.*, glutathione) and inorganic phosphates were used to trigger the release of fluorescein from the G2d2-wrapped nanoparticles. As expected, the ATP

analogues (GTP, UTP, CTP) as well as pyrophosphate (PPi) showed comparable release of fluorescein as observed for ATP, whereas the mono-and biphosphate analogues (AMP and ADP) showed lower drug release (Figure 2C). However, biomolecules like GSH, DNA and BSA commonly found in the cytoplasm showed negligible release of fluorescein, while the trypsin, a typical protease for proteolysis, only induced a 18.3% of release in 24 h, thus indicating the release of the cargo *via* uncapping of the polypeptide is in a "triphosphate-specific" fashion. Additionally, the effect of different pH conditions on the ATP-responsive release was also tested. As shown in Figure 2D, negligible release of fluorescein was observed when the polypeptide wrapped nanoparticles were dispersed in solutions of different pH conditions ranging from 5 to 9 in the absence of ATP, thus demonstrating the robustness of the polypeptide-TDPA-Zn^{2+} complex. However, addition of 5 mM ATP led to a remarkable release of fluorescein at all pH conditions, indicating the pH-independence of the ATP-responsive drug release. Overall, these results demonstrated the successful construction of the proposed polypep-tide-wrapped TDPA-Zn^{2+}-UCNP@MSNs based DDS that possesses ATP-specific stimuli-responsive drug release properties.

Correlating Drug Release from Hybrid Nanoparticle to the Ratiometric Emission Signal of UCNP

After confirming the ATP-specific triggered release properties of the poly-peptide-wrapped TDPA-Zn^{2+}-UCNP@MSNs, we then studied real-time monitoring of drug release using our system. Our UCNPs were rationally designed to have multiple emission peaks in UV to NIR range (Figure 1G). We hypothesized that when anticancer drug (DOX or CPT) was loaded into pores of the UCNP@MSNs (Figure 3A), a LRET between the loaded drugs and UCNP will occur resulting in quenched UV–vis emission of UCNP. However, the NIR emission will remain constant in this scenario (the absorption of the drug typically is in the UV–vis region), thus allowing for long-term tracking and imaging of the drug delivery. Upon ATP-triggered drug release, we expected to observe an enhancement on the UV–vis emission of UCNP due to the elimination of the LRET. As a result, the drug release can be monitored in real-time by monitoring the changes in LRET *via* a ratiometric signal by utilizing the NIR emission of the UCNP as an internal reference.

To verify this hypothesis, G2d2-wrapped nanoparticles loaded with anticancer drugs DOX or CPT were prepared. DOX and CPT have an absorption maximum at 480 and 370 nm, respectively (Figure 3B), which overlaps well with the blue (475 nm) and UV (365 nm) emission of UCNP. As expected, loading with DOX induced a significant quenching of the blue emission while only slightly quenching the UV and green emissions of UCNP (Figure 3C). In contrast, loading with CPT only quenched the UV emission of UCNP (Figure 3D). The absorption wavelength-dependent emission quenching of UCNP strongly indicated the LRET within the drug loaded nanoparticle. This was further supported by observing a shortening in the Tm decay at 451 nm with DOX loading, which demonstrated a dynamic quenching of the Tm emission (Figure S9). In addition to LRET, both DOX and CPT loaded nanoparticles retained the ATP-responsive drug release property. Addition of 1 mM ATP to the drug loaded nanoparticles induced a time dependent release of the encapsulated drug (Figure 3C,D), which was accompanied by a simultaneous luminescence enhancement of UCNP emission. As seen in Figure 3E, there is a linear correlation between the ratiometric

signals of the UCNP emission to the amount of the drug release. On the basis of these results, the time-dependent release profile for DOX and CPT can be established by measurement of the emission of UCNP, thus strongly demonstrating the capability of the proposed DDS for real-time monitoring of drug release kinetics.

Real-Time Monitoring of DOX Release Using Polypeptide Wrapped TDPA-Zn^{2+}-UCNP@MSNs in Cancer Cells

Prior to testing our ATP-responsive DDS *in vitro*, we first evaluated their biocompatibility in cervical cancer cells (HeLa). Our polypeptide wrapped TDPA-Zn^{2+}-UCNP@ MSNs exhibited negligible cytotoxicity in HeLa cells over a wide range of concentrations tested (see Supporting Information, Figure S10). After establishing that our UCNP@MSN-based DDS was indeed biocompatible, we then demonstrated targeted delivery of our UCNP@MSN by using a folic acid (FA) labeled polypeptide.[66] As shown in Figure S11, UCNPs wrapped with FA modified polypeptides can be selectively uptaken by HeLa cells which have been shown to overexpress folate receptors (FRs). In contrast, MCF-7 cells, which lack FR, showed minimal uptake of the nanoparticle. UCNPs without FA ligands were not uptaken by HeLa cells while uptaken in negligible amounts by MCF-7 cells. The differential uptake of our FA-modified UCNPs in HeLa and MCF-7 cells demonstrated the target-specific delivery ability of our UCNP@MSN based DDS.

We further examined its capability in real-time monitoring of the intracellular drug release by incubating the HeLa cells with our UCNPs and monitored their ratiometric upconversion luminescence signals at different time points after incubation. It shown that after 3 h of incubation (Figure 4A–E), the UCNPs showed punctate red emission (656 nm) with negligible blue emissions (475 nm) as well as weak emission for DOX (590 nm), indicating that most of the DDS were entrapped in endosomes at 3 h post incubation and limited amount of DOX was released. This nanoparticle-endosome colocalization was further confirmed by cross-sectional TEM of HeLa cells as shown in Figure S12. However, as time progressed, a time-dependent enhancement of fluorescence intensity (590 nm) coupled with diffuse dispersion of DOX within the cancer cells was obtained, thus demonstrating the ATP-triggered release of DOX from the DDS (Figure 4I,N). Meanwhile, an intracellular diffusion and recovery of UCL signal at 475 nm DDS is clearly detectable, as shown in Figure 4C, H,M. Because of the absence of overlap of DOX absorption with UCL emission at the 656 nm, there is negligible variation in emission intensity within different time points (Figure 4B,G,L), which further confirmed the quantification capability of this DDS using the 656 nm emission as an internal reference, as shown in Figure 3E. The merged images (Figure 4E,J,O) clearly revealed a color change of the cell from red to blue color along the time scale, which strongly suggested that the proposed DDS has the capability of monitoring the drug release in real-time.

CONCLUSIONS

In summary, we have developed an ATP-responsive upconversion nanoparticle-mesoporous silica (UCNP@ MSN)-based DDS with the ability of long-term tracking and real-time monitoring of the drug delivery *in vitro*. The mechanism behind ATP-response is the

competitive binding between multibranched polypeptides and ATP to metallic complex TDPA-Zn^{2+} immobilized on nanoparticle surface. The structural design of polypep-tide and metallic complex allowed for exquisite flexibility for modulating the specificity and sensitivity of this small molecule triggering system. Our developed DDS is biocompatible and can be easily functionalized to achieve additional advantages such as targeted delivery. Moreover, the use of UCNPs in this DDS not only offers a noninvasive approach for long-term tracking of drug delivery by using its NIR excitation (980 nm) and emission (656 nm), but also provides a unique method for real-time monitoring the intra-cellular drug-release kinetics *via* a LRET mechanism combined with a ratiometric signal. The multiemission peaks of UCNP enable the real-time monitoring strategy to be applied to various drugs with different UV–vis absorption properties. Because of the wide availability of ATP in all live cells, especially in the neural stem cells and cancer cells, engineering such a multifunctional ATP-responsive DDS affords great promise for neural stem cell investigation and cancer therapy. It should be noted that the use of high-power 980 nm excitation for UCNP in long-term tracking can potentially cause localized heating, which would result in detrimental effects on biological system. However, construction of a multicolor UCNP with 808 nm NIR light as excitation can enable us to overcome this limitation and further improve the biocompatibility of our DDS.

METHODS

Synthesis of Core–Shell UCNP[61]

(a). Synthesis of β-$NaYF_4$: 30 mol % Yb^{3+}, 0.5 mol % Tm^{3+} Nanoparticles (β-$NaYF_4$:Yb^{3+}/Tm^{3+})—$Y(CH_3CO_2)_3 \cdot xH_2O$ (1.39 mmol), $Yb(CH_3CO_2)_3 \cdot xH_2O$ (0.6 mmol), and $Tm(CH_3CO_2)_3 \cdot xH_2O$ (0.01 mmol) were added to a 100 mL flask containing 12 mL of oleic acid and 15 mL of 1-octadecene. The mixture was heated at 130 °C for 30 min under a vacuum to form the lanthanide-oleate complexes and remove water. Then the solution was cooled to 50 °C naturally under argon. Thereafter, 12 mL of methanol solution containing NH_4F (8 mmol) and NaOH (5 mmol) was added, and the resultant solution was stirred for 30 min. After the methanol was evaporated, the solution was heated to 300 °C (15 °C · min^{-1}) under argon for 90 min and then cooled to RT. The resulting nanoparticles were precipitated by addition of ethanol (30 mL), collected by centrifugation at 1500*g* for 5 min, washed with ethanol several times, and redispersed in 10 mL of hexane.

(b). Synthesis of β-$NaYF_4$: 30 mol % Yb^{3+}, 0.5 mol % Tm^{3+}@β-$NaYF_4$: 18 mol % Yb^{3+}, 2 mol % Er^{3+} Core–Shell Nanoparticles (β-$NaYF_4$:Yb^{3+}/Tm^{3+}@β-$NaYF_4$:Yb^{3+}/Er^{3+})—$Y(CH_3CO_2)_3 \cdot xH_2O$ (1.28 mmol), $Yb(CH_3CO_2)_3 \cdot xH_2O$ (0.288 mmol)), and $Er(CH_3CO_2\text{-})_3 \cdot xH_2O$ (0.032 mmol) were added to a 100 mL flask containing 12 mL of oleic acid and 15 mL of 1-octadecene. The mixture was heated at 130 °C for 30 min under a vacuum to form the lanthanide-oleate complexes and remove water. Then the solution was lowered to 80 °C under argon, and the dispersion of β-$NaYF_4$:Yb^{3+}/Tm^{3+} core nanoparticles in hexanes obtained in last step was added. The resulting solution was heated at 90 °C to remove the hexane. Then the solution was cooled to 50 °C, and 10 mL of methanol solution containing NH_4F (7.2 mmol) and NaOH (4.5 mmol) was added, and the resultant solution was stirred for 30 min. After the methanol was evaporated, the solution

was heated to 300 °C under argon for 90 min and then cooled to RT. The resulting nanoparticles were precipitated by addition of ethanol (20 mL), collected by centrifugation at 1500*g* for 5 min, washed with ethanol several times, and redispersed in 10 mL of hexane.

Synthesis of UCNP@MSNs

In a typical procedure, 40 mg of UCNPs in chloroform (1 mL) were poured into aqueous CTAB solution (10 mL, 360 mg), and the resulting solution was sonicated by using a probe-type sonicator at 400 W for 30 min to result in a transparent UCNPs@CTAB solution. The nanoparticles were collected by centrifugation (13000*g*) and were redispersed in 1 mL of water. The cenctrifugation/redispersion procedure was repeated 3 times to remove the excess amount of CTAB. Thereafter, the UCNP@CTAB solution (1 mL) was added to a CTAB solution (9 mL, 8.2 mg · mL^{-1}) and NaOH solution (0.1 mL, 0.1 M). The mixture was stirred at for 30 min and 50 μL of TEOS was added. The mixture was further stirred at 55 °C for 4 h, and the as-synthesized UCNP@MSNs were collected by centrifugation (7000*g*) and washed with water 3 times.

Synthesis of TDPA-Zn^{2+}/Cu^{2+}-UCNP@MSNs

(a). Boc-TDPA—*Boc*-TDPA was synthesized by a previously reported method.[54] ^{1}H NMR (300 MHz, $CDCl_3$): δ 8.53 (d, J = 4.8 Hz, 4H), 7.61 (t, J = 7.8 Hz, 4H), 7.46 (d, J = 7.8 Hz, 4H), 7.12 (t, J = 5.7 Hz, 4H), 7.01 (s, 2H), 5.23 (d, J = 7.6 Hz, 1H), 4.51 (m, 1H), 3.86 (s, 8H), 3.78 (s, 4H), 3.62 (s, 3H), 2.98 (s, 2H), 1.34 (s, 9H). ESI-MS *m*/*z* cal. 717.86 found 739.9 $[M + Na]^+$.

(b). TDPA-UCNP@MSNs—To the mixture of 70 mg of *Boc*-TDPA and 5 mL of CH_2Cl_2 in ice bathe was added a solution of trifluoroacetic acid (TFA, 1 mL). The mixture was stirred at 4 °C for 30 min and then 1.5 h at RT. The mixture was concentrated in a vacuum and extracted by ethyl acetate. After washed with saturated $NaHCO_3$ and NaCl solution and dried over anhydrous Na_2SO_4, the solution was concentrated to 5 mL in a vacuum. Twenty microliters of 3-(triethoxysiliyl)propyl isocyanate was added to the solution and refluxed overnight. After the solvent was removed, the mixture was added to a toluene-methanol solution (50 mL/3 mL) in which 200 mg of UCNP@MSNs were dispersed and refluxed for overnight. The nanoparticles were collected by centrifugation and washed with methanol for several times, and dried in a vacuum to obtain the TDPA-UCNP@MSNs.

(c). TDPA-Zn^{2+}-UCNP@MSNs—To form the metallic Zn^{2+} chelated complex on TDPA-Zn^{2+} on UCNP@MSNs surface, 100 mg of the TDPA-UCNP@MSNs was dispersed in 3 mL of methanol with 1 mL of 10 mM $Zn(NO_3)$ aqueous solution and stirred for 1 h in RT. The nanoparticles were collected by centrifugation and washed by water for several times. After drying in a vacuum, the TDPA-Zn^{2+}-UCNP@MSNs was obtained as a slight yellow powder.

(d). TDPA-Cu^{2+}-UCNP@MSNs—The TDPA-Cu^{2+}-UCNP@MSNs were prepared by using the same method for TDPA-Zn^{2+}-UCNP@MSNs, while using $CuCl_2$ as metallic source.

Synthesis of Block Polypeptide Poly(Asp-Lys)-*b*-Asp

(a). Synthesis of β-Benzyl ester-L-aspartic acid-N-carboxyanhydride, Asp(OBzl)-NCA.[64]—The Asp(OBzl)-NCA was synthesized by a previously reported method. ^{1}H NMR (400 MHz, DMSO-d_6): δ 8.99 (s, 1H), 7.35–7.38 (m, 5H), 5.13 (s, 2H), 4.69 (t, J = 4.4 Hz, 1H), 3.07 (dd, J = 4.8, 17.6 Hz, 1H), 2.90 (dd, J = 4.0, 18 Hz, 1H).

(b). Synthesis of N-ε-Benzyloxycarbonyl-L-lysine-N-carboxyan-hydride, Lys(Cbz)-NCA.[65]—The Lys(Cbz)-NCA was synthesized by a previously reported method. ^{1}H NMR (300 MHz, DMSO-d_6): δ 9.09 (s, 1H), 7.26–7.38 (m, 5H), 5.01 (s, 2H), 4.40 (t, J = 5.4 Hz, 1H), 2.99 (m, 2H), 1.67–1.74 (m, 2H), 1.32–1.44 (m, 4H).

(c). Synthesis of the First-Generation Tribranched Copolypeptide, G1—The polypeptide was synthesized by using *N*-carboxyanhydride (NCA) based ROMP method. The molar ratio of the two NCA monomers, Asp(OBzl)-NCA and Lys(Cbz)-NCA, was varied to synthesize different polypeptides that will lead to different amounts of branches in final polypeptide products (**G2d**). The following describes the typical procedure for synthesis of a **G1** with a monomer ratio (Asp to Lys) at 3:1.

To a mixture of Asp(OBzl)-NCA (600 mg) and Lys(Cbz)-NCA (183 mg) in 10 mL of anhydrous DMF was added 7.3 mg of tris-(2-aminoethyl)amine (TAEA). The mixture solution was stirred at 45 °C for 72 h under Ar. The polypeptide was precipitated with 20 mL of diethyl ether. The obtained solid was collected by centrifugation and redispersed into 5 mL of THF, which was then added dropwise into a 20 mL of diethyl ether solution to precipitate the polypeptide. After this precipitation-redispersion procedure was repeated for 3 times, the polypeptide was collected and dried under a vacuum. The ratio of Asp to Lys (*x:y*) in this polypeptide was calculated by a fluorescence analysis method, which is described in the below section. ^{1}H NMR (500 MHz, DMSO-d_6): δ 8.18 (CON*H*), 7.16–7.35 [Ar*H*, Asp(OBzl) + Lys (Cbz)], 5.02 [Ar–CH_2, Asp(OBzl) + Lys (Cbz)], 4.64 [α–C*H*, Asp(OBzl)], 4.20 [α–C*H*, Lys(Cbz)], 2.96 [ε–CH_2, Lys(Cbz)], 2.63–2.84 [β–CH_2, Asp(OBzl)], 1.25–1.62 [β, γ and δ–CH_2, Lys(Cbz)]. The signals for CH_2 in TAEA overlap with DMSO-d_6 and H_2O and cannot be isolated.

(d). Synthesis of Polypeptide Core, Gc—Polypeptide core (**Gc**) was obtained through selective deprotection of Lys(Cbz) in polypeptide **G1**. Typically, to 200 mg of **G1** dispersed in 3 mL of TFA was added 0.1 mL of 33% solution of HBr in CH_3COOH. After stirring at RT for 1 h, 5 mL of diethyl ether was added, and the precipitation was isolated *via* centrifugation. The solid was washed with 10 mL of $NaHCO_3$ (0.1 M) and redispersed in 3 mL of THF, which then was added dropwise into 20 mL of diethyl ether solution to precipitate the polypeptide again. The **Gc** was collected and dried under a vacuum. ^{1}H NMR (500 MHz, DMSO-d_6): δ 8.18 (CON*H*), 7.16–7.35 [Ar*H*, Asp(OBzl)], 5.02 [Ar–CH_2, Asp(OBzl)], 4.64 [α–C*H*, Asp(OBzl)], 2.90–3.62 (β–CH_2 for Asp-(OBzl) and CH_2 for TAEA), 2.52–2.88 (ε–CH_2 for Lys), 1.22–1.98 (β, γ and δ–CH_2 for Lys).

(e). Synthesis of the Second-Generation Branched Polypeptide, G2—Multibranched polypeptide **G2** was synthesized using the similar synthetic method for **G1**

with **Gc** as macro initiator and Asp(OBzl)-NCA as monomer. ^{1}H NMR (500 MHz, DMSO-d_6): δ 8.18 (CONH), 7.16–7.35 [ArH, Asp(OBzl)], 5.02 [Ar–CH$_2$, Asp-(OBzl)], 4.64 [α–CH, Asp(OBzl)], 2.90–3.62 (β–CH$_2$ for Asp(OBzl) and CH$_2$ for TAEA), 2.52–2.88 (ε–CH$_2$ for Lys), 1.22–1.78 (β, γ and δ–CH$_2$ for Lys).

(f). Deprotection of the G2 to Achieve the Final Polypeptide, G2d—The polypeptide **G2d** was synthesized by deprotection of **G2**. Typically, 500 mg of **G2** was dispersed in 5 mL mixture of methanol/water (1/1, v/v) by sonication. The solution was mixed with 100 mg of Pd/C (5%) and charged with H_2 under vigorous stirring for 36 h. The mixture was filtered off to obtain a clear solution which was washed with 5 mL of ethyl acetate. The solvent was removed and dried under a vacuum to obtain the polypeptide **G2d***i* (*i* = 1, 2, 3 and 4). ^{1}H NMR (500 MHz, D_2O): 4.62–4.85 (α–CH for Asp, overlap with D_2O), 4.21–4.43 (α–CH Lys), 2.76–3.05 (β–CH$_2$ for Asp), 1.25–1.78 (β, γ, δ–CH$_2$ for Lys).

Preparations of Drug Loaded Nanoparticles

To load drug into the TDPA-Zn^{2+}-UCNP@MSNs, small molecular drugs such as DOX, CPT and model drug fluorescein were stirred together with the nanoparticles in HEPES buffer solution (10 mM, pH 7.4) for 2 h. Thereafter, the nanoparticles were collected by centrifugation (5000*g*) and were redispersed into a HEPES solution of polypeptide (G2d*i*) with sonication. The final drug-loaded polypeptide-wrapped nanoparticles were collected by centrifugation (6000*g*) and repeat washed with water to remove the traces of free drugs and unbound polypeptide.

Characterizations

UV–vis absorption spectra were recorded on a Varian Cary 50 spectrophotometer. Fluorescence spectra were recorded on a Varian Cary Eclipse fluorescence spectrophotometer with an external NIR laser with a wavelength at 980 nm as excitation light source (CNI high power fiber coupled diode laser system, FC-W-980). The total output powers for the lasers are tunable from 1 mW to 10 W. The power density was detected by 1916-R hand-held optical power meter with 818P thermophile detector (Newport Corporation, USA). FT-TR spectra were collected on an Avatar Nicolet FT-IR330 spectrometer. ^{1}H NMR and ^{13}C NMR were acquired on Varian 300/400/500 MHz NMR spectrometer. ESI-MS was collected on Finnigan LCQ DUO LC/MS spectrometer. MALDI-TOF spectrum was recorded on an ABI-MDS SCIEX 4800 MALDI-TOF/TOF mass spectrometer. The DLS size and zeta potential was collected on a Malvern Zetasizer nano S. Transmission electron microscopy (TEM) was performed on a Topcon 002B electron microscope at 200 kV. Sample preparation was carried out by placing a drop of the freshly prepared colloidal solution on a carbon-coated copper grid and allowing the solution to evaporate. Upconversion luminescent/fluorescence imaging of HeLa cells were performed on a Olympus IX83 inverted motorized microscope adapt with an additional external NIR laser with a wavelength at 980 nm as excitation light source (CNI high power fiber coupled diode laser system, FC-W-980, output power is set at 1W).

Cell-Lines and Culture

HeLa cells and MCF-7 cells were used this project. Cells were cultured in the DMEM based medium supplemented with 10% FBS and 1% streptomycin–penicillin. For the delivery experiment, passaged cells were prepared to 40–60% confluency in 24-well plates. After 24 h of plating, media was changed with serum-free basal media (500 μL) and polypeptide-wrapped TDPA-Zn^{2+}-UCNP@MSNs/PEI complexes (20 k, 20 μM, 10 μL) were added. After incubation for 3 h, media was exchanged with normal growth medium.

Measurement of Cytotoxicity

The viabilities of HeLa cells that incubated without or with different concentrations of polypeptide G2d2 wrapped TDPA-Zn^{2+}-UCNP@MSNs were measured by quantifying the cellular ability to reduce the water-soluble tetrazolium dye 3-(4,5-dimethylthiazol-2-yl)-2,5-diphenyl tetrazolium bromide (MTT) to its insoluble formazan salt. Data points were collected in triplicate and expressed as normalized values for control cells (100%).

Imaging of Polypeptide-Warped UCNP@MSN

At different time points following transfection, the cells were imaged using fluorescent microscopy. Upconversion luminescent/fluorescence imaging of cells were preferment on a Olympus IX83 inverted motorized microscope adapt with an external NIR laser with a wavelength at 980 nm as excitation light source (CNI high power fiber coupled diode laser system, FC-W-980, output power is set at 1W).

Supplementary Material

Refer to Web version on PubMed Central for supplementary material.

Acknowledgments

K.-B.L. acknowledges financial support from the NIH Director's Innovator Award [1DP20D006462–01], National Institute of Neurological Disorders and Stroke (NINNDS) [1R21NS085569-01], the NSF 9CHE-1429062 and CBET-12365080, the N.J. Commission on Spinal Cord Grant [CSCR13ERG005], and Busch Biomedical Grant Program.

REFERENCES AND NOTES

1. Mura S, Nicolas J, Couvreur P. Stimuli-Responsive Nanocarriers for Drug Delivery. Nat Mater. 2013; 12:991–1003. [PubMed: 24150417]
2. Kim CS, Duncan B, Creran B, Rotello VM. Triggered Nanoparticles as Therapeutics. Nano Today. 2013; 8:439–447. [PubMed: 24159362]
3. Alarcon CDH, Pennadam S, Alexander C. Stimuli Responsive Polymers for Biomedical Applications. Chem Soc Rev. 2005; 34:276–285. [PubMed: 15726163]
4. Lu Y, Sun WJ, Gu Z. Stimuli-Responsive Nanomaterials for Therapeutic Protein Delivery. J Controlled Release. 2014; 194:1–19.
5. Bansal A, Zhang Y. Photocontrolled Nanoparticle Delivery Systems for Biomedical Applications. Acc Chem Res. 2014; 47:3052–3060. [PubMed: 25137555]
6. Ge ZS, Liu SY. Functional Block Copolymer Assemblies Responsive to Tumor and Intracellular Microenvironments for Site-Specific Drug Delivery and Enhanced Imaging Performance. Chem Soc Rev. 2013; 42:7289–7325. [PubMed: 23549663]

7. Ta T, Porter TM. Thermosensitive Liposomes for Localized Delivery and Triggered Release of Chemotherapy. J Controlled Release. 2013; 169:112–125.
8. Hu JM, Zhang GQ, Liu SY. Enzyme-Responsive Polymeric Assemblies, Nanoparticles and Hydrogels. Chem Soc Rev. 2012; 41:5933–5949. [PubMed: 22695880]
9. Fleige E, Quadir MA, Haag R. Stimuli-Responsive Polymeric Nanocarriers for the Controlled Transport of Active Compounds: Concepts and Applications. Adv Drug Delivery Rev. 2012; 64:866–884.
10. Chen KJ, Liang HF, Chen HL, Wang YC, Cheng PY, Liu HL, Xia YN, Sung HW. A Thermoresponsive Bubble-Generating Liposomal System for Triggering Localized Extracellular Drug Delivery. ACS Nano. 2013; 7:438–446. [PubMed: 23240550]
11. Li ZX, Barnes JC, Bosoy A, Stoddart JF, Zink JI. Mesoporous Silica Nanoparticles in Biomedical Applications. Chem Soc Rev. 2012; 41:2590–2605. [PubMed: 22216418]
12. Vivero-Escoto JL, Huxford-Phillips RC, Lin WB. Silica-Based Nanoprobes for Biomedical Imaging and Theranostic Applications. Chem Soc Rev. 2012; 41:2673–2685. [PubMed: 22234515]
13. Yang PP, Gai SL, Lin J. Functionalized Mesoporous Silica Materials for Controlled Drug Delivery. Chem Soc Rev. 2012; 41:3679–3698. [PubMed: 22441299]
14. Popat A, Hartono SB, Stahr F, Liu J, Qiao SZ, Lu GQ. Mesoporous Silica Nanoparticles for Bioadsorption, Enzyme Immobilisation, and Delivery Carriers. Nanoscale. 2011; 3:2801–2818. [PubMed: 21547299]
15. Wang Y, Wang KY, Zhang R, Liu XG, Yan XY, Wang JX, Wagner E, Huang RQ. Synthesis of Core-Shell Graphitic Carbon@Silica Nanospheres with Dual-Ordered Mesopores for Cancer-Targeted Photothermochemotherapy. ACS Nano. 2014; 8:7870–7879. [PubMed: 25046179]
16. Xiao D, Jia HZ, Zhang J, Liu CW, Zhuo RX, Zhang XZ. A Dual-Responsive Mesoporous Silica Nanoparticle for Tumor-Triggered Targeting Drug Delivery. Small. 2014; 10:591–598. [PubMed: 24106109]
17. Lai JP, Shah BP, Garfunkel E, Lee KB. Versatile Fluorescence Resonance Energy Transfer-Based Mesoporous Silica Nanoparticles for Real-Time Monitoring of Drug Release. ACS Nano. 2013; 7:2741–2750. [PubMed: 23445171]
18. Chen X, Soeriyadi AH, Lu X, Sagnella SM, Kavallaris M, Gooding JJ. Dual Bioresponsive Mesoporous Silica Nanocarrier as an "and" Logic Gate for Targeted Drug Delivery Cancer Cells. Adv Funct Mater. 2014; 24:6999–7006.
19. Chen YW, Chen PJ, Hu SH, Chen IW, Chen SY. NIR-Triggered Synergic Photo-Chemothermal Therapy Delivered by Reduced Graphene Oxide/Carbon/Mesoporous Silica Nanocookies. Adv Funct Mater. 2014; 24:451–459.
20. Jayakumar MKG, Idris NM, Zhang Y. Remote Activation of Biomolecules in Deep Tissues Using Near-Infrared-to-UV Upconversion Nanotransducers. Proc Natl Acad Sci U S A. 2012; 109:8483–8488. [PubMed: 22582171]
21. Lai JP, Mu X, Xu YY, Wu XL, Wu CL, Li C, Chen JB, Zhao YB. Light-Responsive Nanogated Ensemble Based on Polymer Grafted Mesoporous Silica Hybrid Nanoparticles. Chem Commun. 2010; 46:7370–7372.
22. Safari J, Zarnegar Z. Advanced Drug Delivery Systems: Nanotechnology of Health Design a Review. J Saudi Chem Soc. 2014; 18:85–99.
23. Zhang ZX, Balogh D, Wang FA, Sung SY, Nechushtai R, Willner I. Biocatalytic Release of an Anticancer Drug from Nucleic-Acids-Capped Mesoporous SiO_2 Using DNA or Molecular Biomarkers as Triggering Stimuli. ACS Nano. 2013; 7:8455–8468. [PubMed: 23985013]
24. De la Torre C, Mondragon L, Coll C, Sancenon F, Marcos MD, Martinez-Manez R, Amoros P, Perez-Paya E, Orzaez M. Cathepsin-B Induced Controlled Release from Peptide-Capped Mesoporous Silica Nanoparticles. Chem—Eur J. 2014; 20:15309–15314. [PubMed: 25303093]
25. Villalonga R, Diez P, Sanchez A, Aznar E, Martinez-Manez R, Pingarron JM. Enzyme-Controlled Sensing-Actuating Nanomachine Based on Janus Au-Mesoporous Silica Nanoparticles. Chem—Eur J. 2013; 19:7889–7894. [PubMed: 23649789]
26. Li LL, Wang H. Enzyme-Coated Mesoporous Silica Nanoparticles as Efficient Antibacterial Agents *in Vivo*. Adv Healthcare Mater. 2013; 2:1351–1360.

27. Chen ZW, Li ZH, Lin YH, Yin ML, Ren JS, Qu XG. Bioresponsive Hyaluronic Acid-Capped Mesoporous Silica Nanoparticles for Targeted Drug Delivery. Chem—Eur J. 2013; 19:1778–1783. [PubMed: 23303570]
28. Popat A, Ross BP, Liu J, Jambhrunkar S, Kleitz F, Qiao SZ. Enzyme-Responsive Controlled Release of Covalently Bound Prodrug from Functional Mesoporous Silica Nanospheres. Angew Chem, Int Ed. 2012; 51:12486–12489.
29. Zhou YF, Tozzi F, Chen JY, Fan F, Xia L, Wang JR, Gao G, Zhang AJ, Xia XF, Brasher H, et al. Intracellular ATP Levels are a Pivotal Determinant of Chemoresistance in Colon Cancer Cells. Cancer Res. 2012; 72:304–314. [PubMed: 22084398]
30. Beis I, Newsholme EA. The Contents of Adenine Nucleotides, Phosphagens and Some Glycolytic Intermediates in Resting Muscles from Vertebrates and Invertebrates. Biochem J. 1975; 152:23–32. [PubMed: 1212224]
31. Sperlagh B, Vizi ES. Neuronal Synthesis, Storage and Release of ATP. Semin Neurosci. 1996; 8:175–186.
32. He XX, Zhao YX, He DG, Wang KM, Xu FZ, Tang JL. ATP-Responsive Controlled Release System Using Aptamer-Functionalized Mesoporous Silica Nanoparticles. Langmuir. 2012; 28:12909–12915. [PubMed: 22889263]
33. Mo R, Jiang TY, DiSanto R, Tai WY, Gu Z. ATP-Triggered Anticancer Drug Delivery. Nat Commun. 2014; 5:3364. [PubMed: 24618921]
34. Mo R, Jiang TY, Gu Z. Enhanced Anticancer Efficacy by ATP-Mediated Liposomal Drug Delivery. Angew Chem, Int Ed. 2014; 53:5815–5820.
35. Myhr G. Multimodal Cancer Treatment: Real Time Monitoring, Optimization, and Synergistic Effects. Technol Cancer Res Treat. 2008; 7:409–414. [PubMed: 18783293]
36. Probst CE, Zrazhevskiy P, Bagalkot V, Gao XH. Quantum Dots as a Platform for Nanoparticle Drug Delivery Vehicle Design. Adv Drug Delivery Rev. 2013; 65:703–718.
37. Panikkanvalappil SR, Mahmoud MA, Mackey MA, El-Sayed MA. Surface-Enhanced Raman Spectroscopy for Real-Time Monitoring of Reactive Oxygen Species-Induced DNA Damage and Its Prevention by Platinum Nanoparticles. ACS Nano. 2013; 7:7524–7533. [PubMed: 23952174]
38. Ock K, Jeon WI, Ganbold EO, Kim M, Park J, Seo JH, Cho K, Joo SW, Lee SY. Real-Time Monitoring of Glutathione-Triggered Thiopurine Anticancer Drug Release in Live Cells Investigated by Surface-Enhanced Raman Scattering. Anal Chem. 2012; 84:2172–2178. [PubMed: 22280519]
39. Fernando R, Downs J, Maples D, Ranjan A. MRI-Guided Monitoring of Thermal Dose and Targeted Drug Delivery for Cancer Therapy. Pharm Res. 2013; 30:2709–2717. [PubMed: 23780716]
40. Liu JN, Bu WB, Pan LM, Zhang S, Chen F, Zhou LP, Zhao KL, Peng WJ, Shi JL. Simultaneous Nuclear Imaging and Intranuclear Drug Delivery by Nuclear-Targeted Multifunctional Upconversion Nanoprobes. Biomaterials. 2012; 33:7282–7290. [PubMed: 22796158]
41. Liu JN, Bu JW, Bu WB, Zhang SJ, Pan LM, Fan WP, Chen F, Zhou LP, Peng WJ, Zhao KL, et al. Real-Time *in Vivo* Quantitative Monitoring of Drug Release by Dual-Mode Magnetic Resonance and Upconverted Luminescence Imaging. Angew Chem, Int Ed. 2014; 53:4551–4555.
42. Saeed M, Saloner D, Weber O, Martin A, Henk C, Higgins C. MRI in Guiding and Assessing Intramyocardial Therapy. Eur Radiol. 2005; 15:851–863. [PubMed: 15856250]
43. Tagami T, Foltz WD, Ernsting MJ, Lee CM, Tannock IF, May JP, Li SD. MRI Monitoring of Intratumoral Drug Delivery and Prediction of the Therapeutic Effect with a Multifunctional Thermosensitive Liposome. Biomaterials. 2011; 32:6570–6578. [PubMed: 21641639]
44. Jana A, Nguyen KT, Li X, Zhu PC, Tan NS, Agren H, Zhao YL. Perylene-Derived Single-Component Organic Nanoparticles with Tunable Emission: Efficient Anticancer Drug Carriers with Real-Time Monitoring of Drug Release. ACS Nano. 2014; 8:5939–5952. [PubMed: 24824959]
45. Qiu F, Wang DL, Zhu Q, Zhu LJ, Tong GS, Lu YF, Yan DY, Zhu XY. Real-Time Monitoring of Anticancer Drug Release with Highly Fluorescent Star-Conjugated Copolymer as a Drug Carrier. Biomacromolecules. 2014; 15:1355–1364. [PubMed: 24606561]

46. Gui RJ, Wan AJ, Zhang YL, Li HL, Zhao TT. Ratiometric and Time-Resolved Fluorimetry from Quantum Dots Featuring Drug Carriers for Real-Time Monitoring of Drug Release *in Situ*. Anal Chem. 2014; 86:5211–5214. [PubMed: 24827984]
47. Tang J, Kong B, Wu H, Xu M, Wang YC, Wang YL, Zhao DY, Zheng GF. Carbon Nanodots Featuring Efficient FRET for Real-Time Monitoring of Drug Delivery and Two-Photon Imaging. Adv Mater. 2013; 25:6569–6574. [PubMed: 23996326]
48. Yang YM. Upconversion Nanophosphors for Use in Bioimaging, Therapy, Drug Delivery and Bioassays. Microchim Acta. 2014; 181:263–294.
49. Nguyen PD, Son SJ, Min J. Upconversion Nanoparticles in Bioassays, Optical Imaging and Therapy. J Nanosci Nanotechnol. 2014; 14:157–174. [PubMed: 24730257]
50. Chen F, Bu W, Cai W, Shi J. Functionalized Upconver-sion Nanoparticles: Versatile Nanoplatforms for Translational Research. Curr Mol Med. 2013; 13:1613–1632. [PubMed: 24206131]
51. Lai JP, Zhang YX, Pasquale N, Lee KB. An Upconversion Nanoparticle with Orthogonal Emissions Using Dual NIR Excitations for Controlled Two-Way Photoswitching. Angew Chem, Int Ed. 2014; 53:14419–14423.
52. Chen GY, Qju HL, Prasad PN, Chen XY. Upconversion Nanoparticles: Design, Nanochemistry, and Applications in Theranostics. Chem Rev. 2014; 114:5161–5214. [PubMed: 24605868]
53. Hirayama T, Taki M, Kodan A, Kato H, Yamamoto Y. Selective Labeling of Tag-Fused Protein by Tryptophan-Sensitized Luminescence of a Terbium Complex. Chem Commun. 2009:3196–3198.
54. Ojida A, Honda K, Shinmi D, Kiyonaka S, Mori Y, Hamachi I. Oligo-Asp Tag/Zn(II) Complex Probe as a New Pair for Labeling and Fluorescence Imaging of Proteins. J Am Chem Soc. 2006; 128:10452–10459. [PubMed: 16895410]
55. Nonaka H, Fujishima S, Uchinomiya S, Ojida A, Hamachi I. Selective Covalent Labeling of Tag-Fused GPCR Proteins on Live Cell Surface with a Synthetic Probe for Their Functional Analysis. J Am Chem Soc. 2010; 132:9301–9309. [PubMed: 20568758]
56. Jiang S, Zhang Y. Upconversion Nanoparticle-Based FRET System for Study of siRNA in Live Cells. Langmuir. 2010; 26:6689–6694. [PubMed: 20073488]
57. Li ZQ, Zhang Y, Jiang S. Multicolor Core/Shell-Structured Upconversion Fluorescent Nanoparticles. Adv Mater. 2008; 20:4765–4769.
58. Gorris HH, Ali R, Saleh SM, Wolfbeis OS. Tuning the Dual Emission of Photon-Upconverting Nanoparticles for Ratiometric Multiplexed Encoding. Adv Mater. 2011; 23:1652–1655. [PubMed: 21472793]
59. Ojida A, Takashima I, Kohira T, Nonaka H, Hamachi I. Turn-on Fluorescence Sensing of Nucleoside Polyphosphates Using a Xanthene-Based Zn(II) Complex Chemo-sensor. J Am Chem Soc. 2008; 130:12095–12101. [PubMed: 18700758]
60. Ojida A, Nonaka H, Miyahara Y, Tamaru SI, Sada K, Hamachi I. Bis(Dpa-Zn-II) Appended Xanthone: Excitation Ratiometric Chemosensor for Phosphate Anions. Angew Chem, Int Ed. 2006; 45:5518–5521.
61. Boyer JC, Carling CJ, Gates BD, Branda NR. Two-Way Photoswitching Using One Type of Near-Infrared Light, Upconverting Nanoparticles, and Changing Only the Light Intensity. J Am Chem Soc. 2010; 132:15766–15772. [PubMed: 20949969]
62. Ojida A, Fujishima S, Honda K, Nonaka H, Uchinomiya S, Hamachi I. Binuclear Ni-II-DpaTyr Complex as a High Affinity Probe for an Oligo-Aspartate Tag Tethered to Proteins. Chem —Asian J. 2010; 5:877–886. [PubMed: 20143369]
63. Kricheldorf HR. Polypeptides and 100 Years of Chemistry of α-Amino Acid *N*-Carboxyanhydrides. Angew Chem, Int Ed. 2006; 45:5752–5784.
64. Wilder R, Mobashery S. The Use of Triphosgene in Preparation of *N*-Carboxy-α-Amino Acid Anhydrides. J Org Chem. 1992; 57:2755–2756.
65. Klok HA, Rodriguez-Hernandez J. Dendritic-Graft Polypeptides. Macromolecules. 2002; 35:8718–8723.
66. Feng D, Song YC, Shi W, Li XH, Ma HM. Distinguishing Folate-Receptor-Positive Cells from Folate-Receptor-Negative Cells Using a Fluorescence Off-On Nanoprobe. Anal Chem. 2013; 85:6530–653. [PubMed: 23751075]

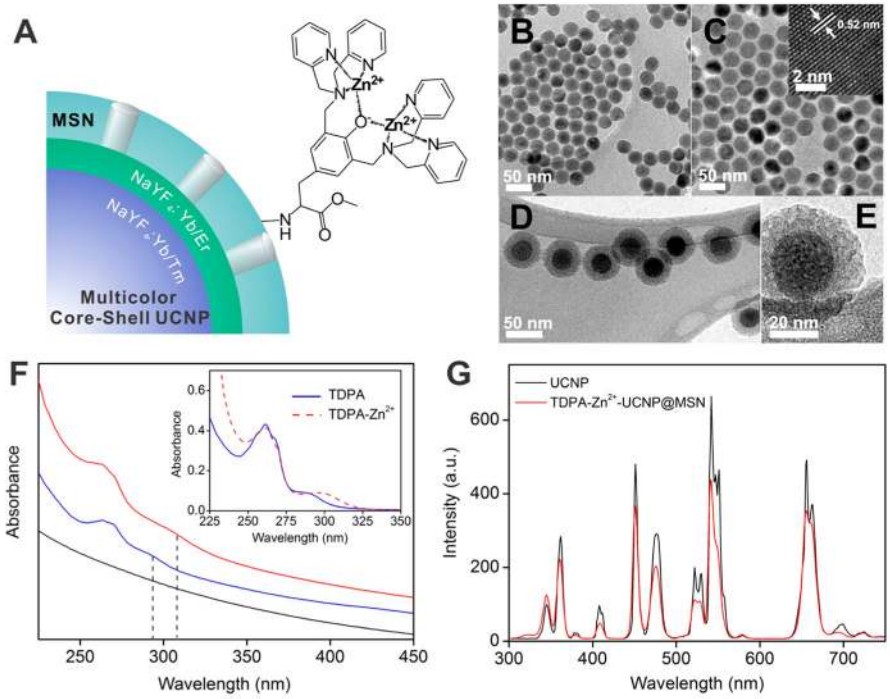

Figure 1.

(A) Structural illustration of core–shell TDPA-Zn^{2+}-UCNP@MSN. (B) TEM characterization of the UCNP core, β-$NaYF_4$: Yb^{3+}/Tm^{3+} and (C) after growth of a $NaYF_4$:Yb^{3+}/Er^{3+} shell. The inset of (B) shows the HR-TEM image of (100) crystallographic planes of the UCNP, confirming the hexagonal phase. (D,E) TEM characterization of the TDPA-Zn^{2+}-UCNP@MSNs clearly revealed the core–shell nanoparticle with a mesoporous silica shell. (F) UV–vis absorption spectrum of the UCNP@MSNs (black line), TDPA-UCNP@MSNs (blue line) and TDPA-Zn^{2+}-UCNP@MSNs (red line) in HEPES buffer solution (pH 7.4, 10 mM). The appearance of the characteristic absorption peak of TDPA at 270 and 290 nm indicated the successful conjugation of TDPA to the nanoparticle surface. The successful chelating of TDPA with Zn^{2+} to form metallic complex was confirmed by obtaining a red-shift of the peak at 290 to 312 nm, a similar spectral change observed in the formation of TDPA-Zn^{2+} complex (25 μM) in HEPES solution, as shown in the inset. (G) Upconversion luminescence of the UCNP (1 wt % in cyclohexane) and TDPA-Zn^{2+}-UCNP@MSN (5 wt % in HEPES buffer, pH 7.4, 10 mM) with an excitation at 980 nm (80 $W \cdot cm^{-2}$).

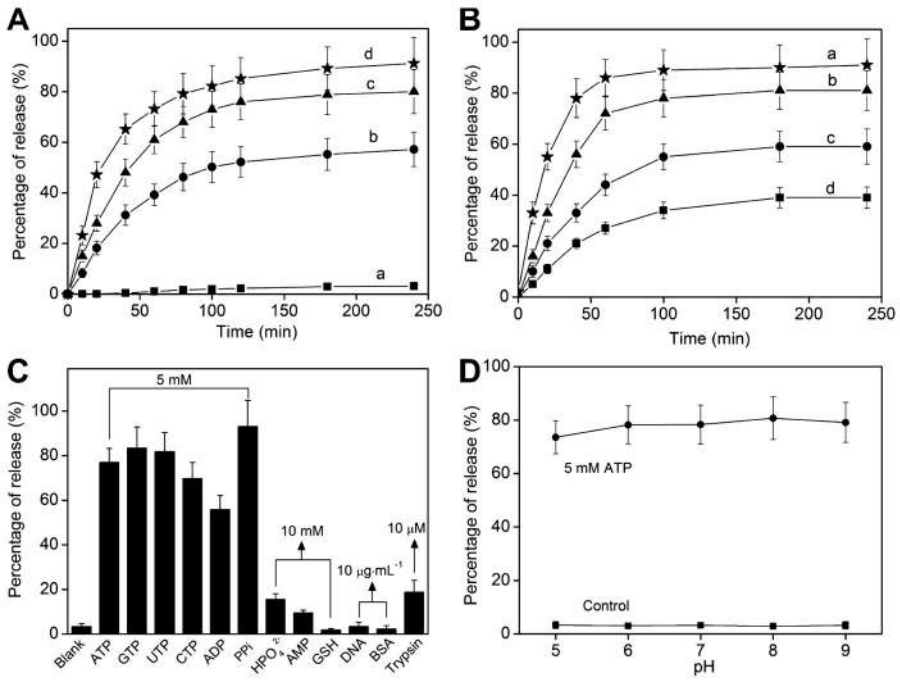

Figure 2.

(A) Model drug fluorescein release profile of polypeptide G2d2-wrapped TDPA-Zn^{2+}-UCNP@MSNs in HEPES solution in the presence of different amount of ATP: a, 0; b, 1 mM; c, 5 mM; and d 10 mM. (B) Release of fluorescein from TDPA-Zn^{2+}-UCNP@MSNs wrapped with different peptides in HEPEs solution in the presence of 5 mM ATP. a, G2d1; b, G2d2; c, G2d3; d, G2d4. (C) Release of fluorescein from G2d2-wrapped TDPA-Zn^{2+}-UCNP@MSN in response to various biomolecules, indicates the specific binding of the polypeptide wrapped nanoparticles for ATP and its analogues. Nanoparticle is 0.2 wt % dispersion in 10 mM pH 7.4 HEPES buffer solution. Various biomolecules were added to the nanoparticles solution and incubated for 4 h to monitor the release of fluorescein, except that trypsin was incubated with nanoparticles solution at 37 °C for 24 h. (D) Fluorescein release from G2d2-wrapped TDPA-Zn^{2+}-UCNP@MSNs at different pHs in the absence and presence of 5 mM ATP. pH was adjusted using 0.1 M NaOH and 0.1 M HCl solution.

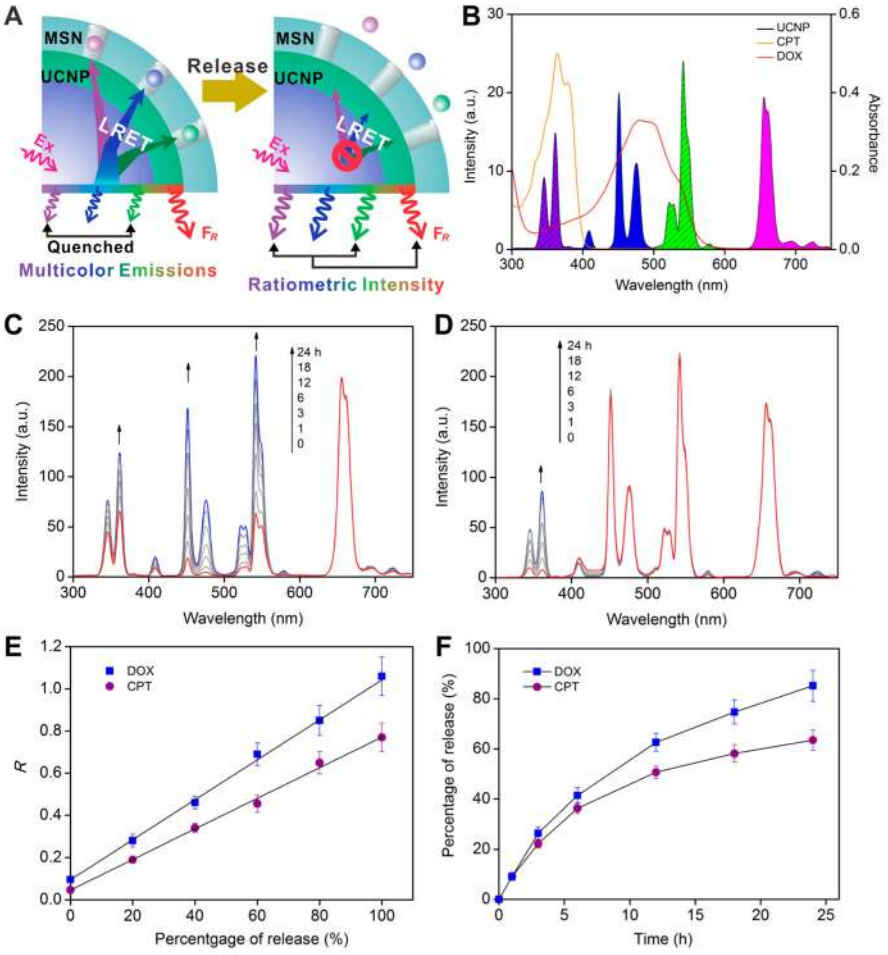

Figure 3.

(A) Schematic illustration of the working mechanism for the real-time monitoring of drug release using the proposed polypeptide-wrapped multicolor TDPA-Zn^{2+}-UCNP@MSN. (B) Spectrum overlaps between the UV–vis absorption of anticancer drug DOX (30 μM in water) and CPT (20 M in methanol), and the emission of the core–shell UCNP@MSN (5 wt % in HEPES buffer). (C–D) Time dependent emission spectrum of the G2d2-wrapped TDPA-Zn^{2+}-UCNP@MSNs load with DOX and CPT, respectively, in HEPES solution in the presence of 5 mM ATP. Concentration for nanoparticle is 0.2 wt %. The enhancement in the UV–vis emission indicated the progressive release of encapsulated anticancer drugs. (E) Linear relationships between the amount of drugs released and the ratiometric signal (R) of the UCNP, where the R for DOX is the ratio of I_{472nm} to I_{656nm}, and R for CPT is the ratio of I_{365nm} to I_{656nm}. The power density of 980 nm excitation was kept at 80 W · cm^{-2}. (F) Time-dependent release profiles for DOX and CPT monitored by using the ratiometric signal of UCNP.

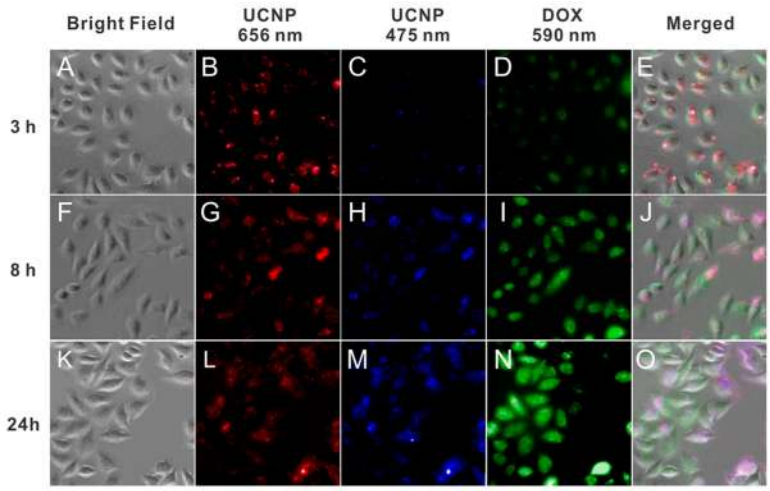

Figure 4.

Fluorescence microscopy images depicting the change in emission signal of UCNP and DOX in HeLa cells treated with polypeptide G2d2-wrapped TDPA-Zn^{2+}-UCNP@MSNs at 3, 8, and 24 h after incubation.

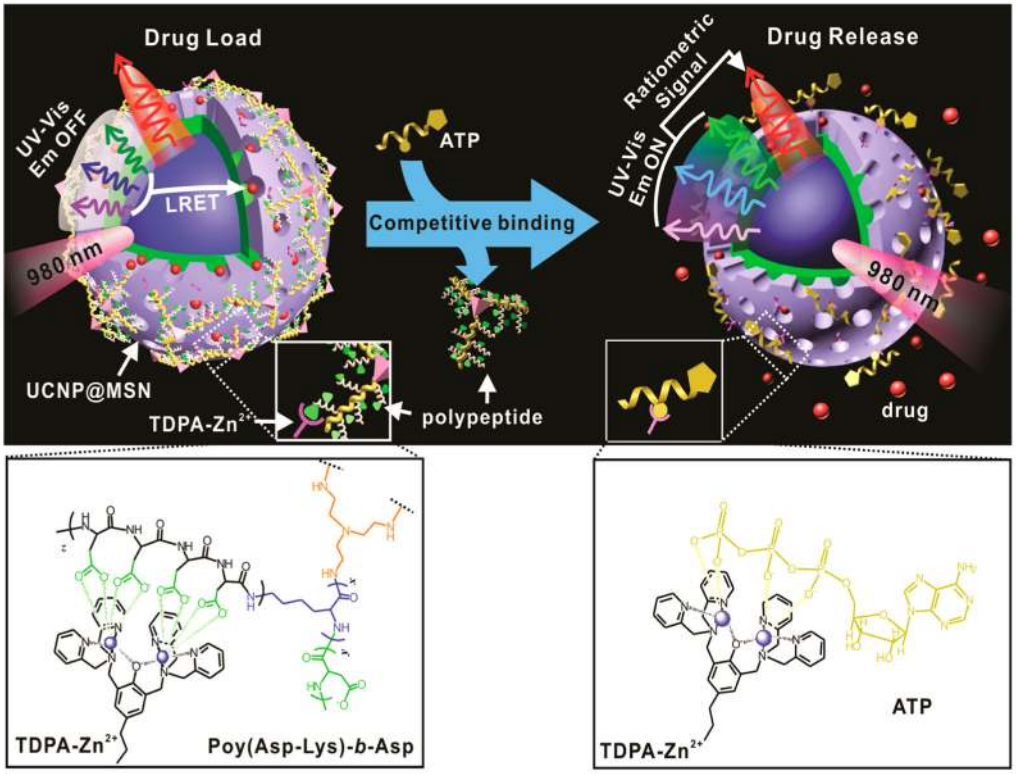

Scheme 1.

Schematic representation of the real-time monitoring of ATP-responsive drug release from polypeptide wrapped TDPA-Zn^{2+}-UCNP@MSNs. Small molecule drugs were entrapped within the mesopores of the silica shell on the hybrid nanoparticle by branched polypeptide capping the pores through a multivalent interaction between the oligo-aspartate side chain in the polypeptide and the TDPA-Zn^{2+} complex on nanoparticles surface. The UV–vis emission from the multicolor UCNP under 980 nm excitation was quenched because of the LRET between the loaded drugs and the UCNP. Addition of small molecular nucleoside-polyphosphates such as ATP led to a competitive binding of ATP to the TDPA-Zn^{2+} complex, which displaced the surface bound compact polypeptide because of the high binding affinity of ATP to the metallic complex. The drug release was accompanied with an enhancement in the UV–vis emission of UCNP, which allows for real-time monitoring of the drug release *via* a ratiometric signal using the NIR emission of UCNP as an internal reference.

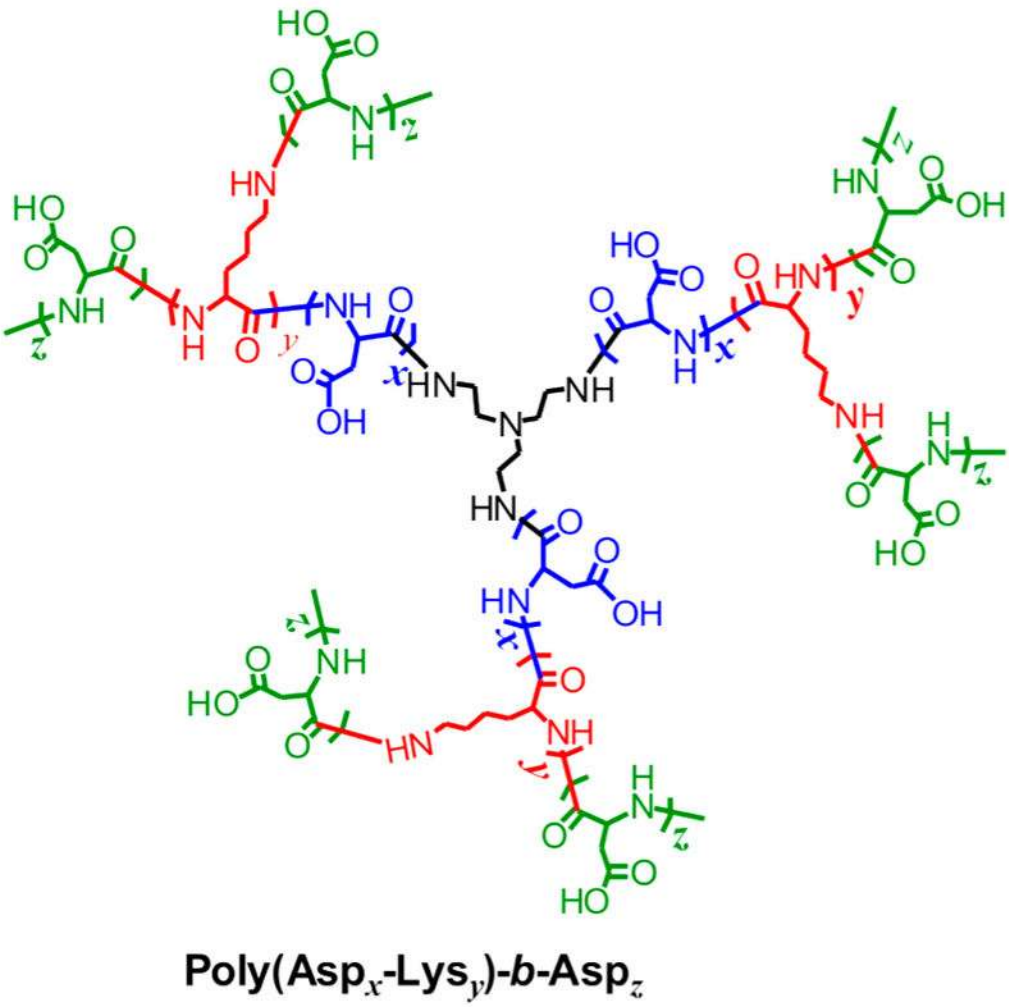

Scheme 2.
Molecular structure of G2d, poly(Asp-Lys)-*b*-Asp.

TABLE 1

Mean Molecular Weight and Composition of the Synthesized Polypeptides

polypeptide	M_w (g/mol)[a]	x, y, z[a]	x:y[b]
G2d1	6382	6, 1, 5	7:1
G2d2	10335	6, 1, 11	7:1
G2d3	8346	5, 2, 5	3:1
G2d4	12750	5, 2, 10	3:1

[a]Determined by fluorescamine based fluorescence assay.

[b]Determined by ^{1}H NMR. Only the ratio *x:y* can be obtained. For more details, see Supporting Information.